Journal Renewable Energy 9[21]1-12: e20921112
Article

Análisis comparativo de colectores solares de placa plana evacuados bajo condiciones limpias y de ensuciamiento

Comparative analysis of evacuated flat plate solar collectors under clean and fouled conditions

Lugo-Granados, Hebert Gerardo*[a], Canizalez-Dávalos, Lázaro[b] and Picón-Núñez, Martín[c]

[a] Autonomous University of Zacatecas • F-2050-2019 • 0000-0002-0027-3418 • 487049
[b] Autonomous University of Zacatecas • ABW-3215-2022 • 0000-0002-3126-8574 • 164509
[c] University of Guanajuato • AHA-5481-2022 • 0000-0002-0793-192X • 12408

SECIHTI classification:

Area: Engineering
Field: Engineering
Discipline: Mechanical Engineering
Subdiscipline: Thermal Engineering

https://doi.org/10.35429/JRE.2025.9.21.2.1.12
Article History:
Received: June 20, 2025
Accepted: December 05, 2025

* ✉ [lugh871024@gmail.com]

Abstract

This study evaluates the thermal performance of two configurations of evacuated flat-plate solar collectors: serpentine-type and parallel-type, under both clean conditions and fouling caused by calcium carbonate ($CaCO_3$) scaling. The aim is to determine which of the two technologies offers higher efficiency and requires fewer units to achieve an outlet temperature of 90 °C. Results indicate that parallel collectors reach a higher thermal efficiency (0.80 compared to 0.76 for the serpentine configuration) and require fewer units to attain the target temperature. In the presence of scaling, 20 parallel collectors are needed, compared to 23 in the serpentine arrangement — representing a 15% increase in the number of collectors required. These findings suggest that the parallel configuration not only enhances thermal performance but also offers a more cost-effective and efficient solution.

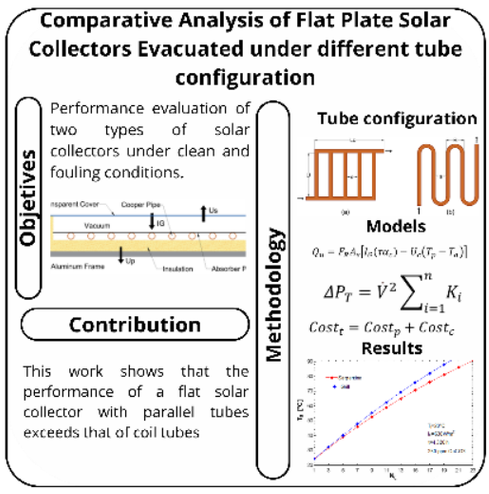

Evacuated Solar Collector, Parallel Tubes, Serpentine Tubes

Resumen

Este estudio evalúa el desempeño térmico de dos configuraciones de colectores solares planos evacuados: tipo serpentín y tipo paralelo, tanto en condiciones limpias como bajo ensuciamiento por incrustaciones de carbonato de calcio ($CaCO_3$). El objetivo es determinar cuál de las dos tecnologías ofrece mayor eficiencia y menor requerimiento de equipos para alcanzar una temperatura de salida de 90 °C. Los resultados muestran que los colectores en paralelo alcanzan una eficiencia térmica superior (0.80 frente a 0.76 del serpentín) y requieren menos unidades para lograr dicha temperatura. En presencia de incrustaciones, se necesitan 20 colectores en paralelo, comparados con 23 en configuración serpentín, lo que implica un aumento del 15 % en el número de colectores requeridos. Estos hallazgos sugieren que la configuración en paralelo no solo mejora el rendimiento térmico, sino que también representa una opción más rentable y eficiente.

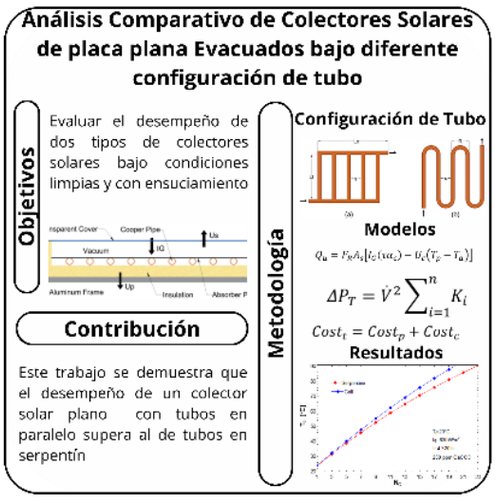

Colector Solar evacuado, tubos en Paralelo, Tubos en Serpentín

Area: Dissemination and universal access to science

Citation: Lugo-Granados, Hebert Gerardo, Canizalez-Dávalos, Lázaro and Picón-Núñez, Martín. [2025]. Análisis comparativo de colectores solares de placa plana evacuados bajo condiciones limpias y de ensuciamiento. Journal Renewable Energy. 9[21] 1-12: e10921112.

1. Introduction

The growing need to adopt renewable energy sources has driven the development of more efficient solar thermal technologies. Solar thermal energy offers a sustainable and effective means of generating heat for residential, commercial, and industrial applications. Among the most commonly used technologies are flat plate collectors (FPC) and evacuated tube collectors (ETC), both of which convert solar radiation into thermal energy with notable efficiency (Kalogirou, 2004).

In a comparative study, Ayompe et al. (2011) demonstrated that evacuated tube collectors outperform flat plate collectors in terms of efficiency. By combining both technologies, the evacuated flat plate collector (EFPC) emerges, harnessing the advantages of each type. However, despite their high efficiency, EFPCs are not yet widely available on the market. It is therefore necessary to explore new designs that enhance durability and performance, while reducing operational and investment costs (Kalair et al., 2022).

Beyond design considerations, the performance of these systems depends on factors such as materials, thermal fluid, operating conditions, and, crucially, the hydraulic flow configuration (Pandey et al., 2017). Whether configured as a coil or in parallel, the flow arrangement directly influences thermo-hydraulic performance.

Gao et al. (2020) developed a solar thermal system using optimised evacuated flat plate collectors designed to operate at medium temperatures. They achieved a peak thermal efficiency of 59.6% and an outlet temperature of 123 °C under solar irradiance of 835.2 W/m². Similarly, Hassan et al. (2023) evaluated an evacuated flat plate collector with spiral tubes, using a water-glycol mixture as the thermal fluid. Their system reached a maximum efficiency of 78% and temperatures of up to 98 °C. In another study, Deng and Zhao (2013) analysed a flat solar collector incorporating microchannels and heat-pipe tubes (MHPA-FPC), highlighting its rapid thermal response and effective temperature distribution. The system achieved an instantaneous peak efficiency of 80%. Numerous studies have examined the performance of solar collectors under various configurations and climatic conditions.

However, most have focused on ideal scenarios, without accounting for the impact of mineral scaling. It is therefore essential to assess the thermal, hydraulic, and economic behaviour of these systems under scaling conditions, to establish technical criteria for more robust and efficient designs.

Scaling is one of the principal challenges in the long-term operation of solar collectors, particularly in regions with high water hardness. The accumulation of mineral salts reduces thermal efficiency, increases pressure drop, and raises pumping costs (Bott, 1995). In recent years, Lugo Granados et al. (2023) demonstrated that reducing the free flow area by 40% significantly decreases scale formation without compromising thermal performance. Subsequently, Lugo Granados et al. (2024) evaluated the redesign of collector networks under scaling conditions, concluding that existing systems can be reconfigured using flow velocity as a key parameter to mitigate fouling.

To address these effects, several solutions have been proposed, including the use of water-glycol mixtures and nanofluids, which may enhance thermal efficiency by 5% to 35% compared to conventional fluids. However, their application presents limitations. Nanoparticle sedimentation can reduce heat transfer by up to 11%, increase viscosity, and lead to greater hydraulic losses (García-Rincón & Flores-Prieto, 2024). Although Bocanegra et al. (2025) highlight the improved optical and thermal properties of nanofluids, colloidal stability remains a challenge for long-term use. For instance, Deshmukh et al. (2025) reported an efficiency of up to 80.47% using titanium nitride (TiN) nanofluids and twisted tape inserts, but with a 64% increase in pressure drop and higher pumping requirements.

Box 1

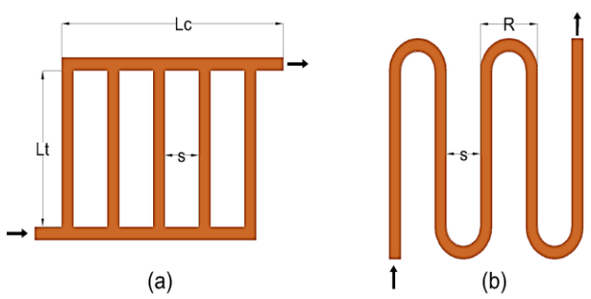

Figure 1
Internal tube layout within the solar collector: a) parallel configuration, b) spiral configuration
Source: Own Elaboration

ISSN: 2523-6881
RENIECYT-SECIHTI: 1702902

Lugo-Granados, Hebert Gerardo, Canizalez-Dávalos, Lázaro and Picón-Núñez, Martín. [2025]. Análisis comparativo de colectores solares de placa plana evacuados bajo condiciones limpias y de ensuciamiento. Journal Renewable Energy. 9[21] 1-12: e10921112.
https://doi.org/10.35429/JRE.2025.9.21.2.1.12

The use of nanofluids or water-glycol mixtures presents significant limitations, notably their high cost, which restricts their application in large-scale solar systems or in regions with limited resources. For these technical and economic reasons, this study focuses on the use of water as the thermal fluid, with particular emphasis on analysing scaling-related fouling which can lead to the development of cleaning strategies based on the prediction of scale formation over time. The objective of this work is to compare the performance of flat-plate solar collectors with evacuated tubes under two hydraulic configurations: serpentine and parallel (Figures 1 and 2). Both clean and fouled conditions are evaluated, considering key variables such as thermal efficiency, useful energy output, pressure drop, and operational costs. The results will help identify the most suitable configuration for environments with high water hardness and provide recommendations for implementing more efficient and sustainable solar thermal systems.

Box 2

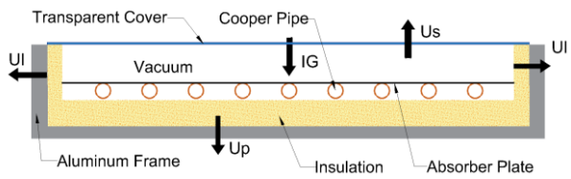

Figure 2
Evacuated flat-plate solar collector.
Source: Own Elaboration

2. Methodology

The methodology of this study aims to compare the thermal, hydraulic, and economic performance of two configurations of evacuated flat-plate solar collectors: one with tubes arranged in parallel, and the other featuring a serpentine-shaped tube. The analysis is conducted under clean conditions as well as considering the impact of scaling-related fouling.

2.1 Thermohydraulic Model:

Mathematical models were adapted to simulate the thermal and hydraulic behaviour of both configurations. These models incorporate parameters such as pressure drop, thermal efficiency, heat transfer coefficients, and head loss, following the approach proposed by Duffie & Beckman (2013).

The properties of the thermal fluid (water) and local climatic conditions were considered to represent realistic scenarios. The amount of useful heat Qu (W) absorbed by a solar collector depends on the incident solar radiation IG (W/m²), the cover transmittance (τ), the plate absorptance (α), and thermal losses, represented by the overall heat loss coefficient Uc (W/m²·°C) and the temperature difference between the absorber plate Tp (°C) and the ambient Ta (°C). This useful energy is adjusted by the heat removal factor (FR), which indicates how efficiently the heat is transferred to the fluid, and by the collector area, As (m²). This relationship is expressed in Equation (1):

$$Q_u = F_R A_s \left[I_G (\tau \alpha_c) - U_c \left(T_p - T_a \right) \right] \quad (1)$$

Figure 3 illustrates the thermal model representing the relationship between the absorber plate temperature T_{pm} (°C) and the ambient temperature T_a (°C). The overall heat loss coefficient U_C (W/m²°C) combines three components: the top loss coefficient U_s (W/m²°C), the back loss coefficient U_P (W/m²°C), and the side loss coefficient U_l (W/m²°C), as shown in Eq (2).

$$U_c = U_s + U_p + U_l \quad (2)$$

Heat loss from the top of the collector arises from convection and radiation between the absorber plate and the cover. The top loss coefficient (Us)is calculated as the inverse of the sum of two internal thermal resistances: R1 (°C/W) and R2 (W/m·°C), as shown in Equation (3).

The thermal resistance R1 (Equation 4) represents heat transfer between the absorber plate and the ambient, accounting for both convection (hc_{c-a}) and radiation (hr_{c-a}).

ISSN: 2523-6881
RENIECYT-SECIHTI: 1702902

Lugo-Granados, Hebert Gerardo, Canizalez-Dávalos, Lázaro and Picón-Núñez, Martín. [2025]. Análisis comparativo de colectores solares de placa plana evacuados bajo condiciones limpias y de ensuciamiento. Journal Renewable Energy. 9[21] 1-12: e10921112.
https://doi.org/10.35429/JRE.2025.9.21.2.1.12

Box 3

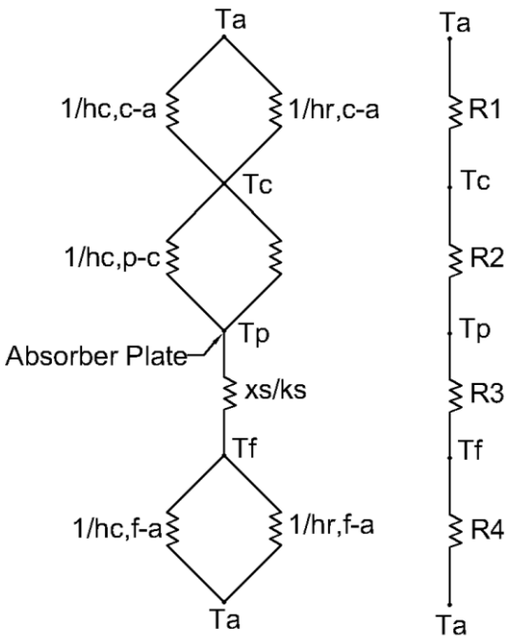

Figure 3
Heat transfer resistances within the solar collector.
Source: Own elaboration

In contrast, resistance R2 (Equation 5) corresponds to the space between the plate and the cover, where heat is transferred solely by radiation (hr_{p-c}), a characteristic feature of evacuated collectors.

$$U_s = \frac{1}{R_1+R_2} \quad (3)$$

$$R_1 = \frac{1}{hr_{c-a} + hc_{c-a}} \quad (4)$$

$$R_2 = \frac{1}{hr_{p-c}} \quad (5)$$

The back loss coefficient (U_p) depends on thermal resistances due to conduction through the insulation (R_3(°C/W)) and from combined convection and radiation (R_4 (°C/W)) between the backplate and the surroundings, Eq(6). As (R_4) is negligible compared to (R_3), its effect is typically ignored (Eq (8)). Here, ks (W/m °C) is the thermal conductivity and xs (m) is the thickness of the back insulation material.

$$U_p = \frac{1}{R_3+R_4} \quad (6)$$

$$R_3 = \frac{k_s}{x_s} \quad (7)$$

$$R_4 = \frac{1}{hr_{f-a} + hc_{f-a}} \quad (8)$$

The side heat loss coefficient (U_l) is derived considering one-dimensional thermal flux across the system perimeter and referenced to the total collector area (A_c), as shown in Eq(9). Where A_c is the collector surface area, x_l is the side insulation thickness, p and h are the perimeter and the height of the collector.

$$U_l = \left(\frac{k_s}{x_l}\right) \cdot \left(\frac{p\ h}{A_c}\right) \quad (9)$$

The heat removal factor (F_R) described in Eq(10), is a function of the mass flow rate $\dot{m}_f$ (kg/s), and the efficiency factor of the collector. The term F´ in Eq(11) is a function of the tube spacing S (m), the inner diameter di (m) and outer diameter do (m) of the tubes, and the resistance to heat transfer from the absorber plate to the working fluid. It also includes the resistance arising from convection between the inner tube wall and the working fluid Rh (m^2°C/W). The resistance due to the tube wall Rt (m^2°C/W) and the fouling layer resistance Rs (m^2°C/W). Cb (m^2°C/W) is the resistance caused by the tube/plate bond and is described in Eq(12).

$$F_{R,\theta} = \frac{\dot{m}_f Cp_f}{A_s U_c}\left[1 - e^{\frac{-A_s U_c F'}{\dot{m}_f Cp_f}}\right] \quad (10)$$

$$F' = \frac{1/U_c}{S\left[\frac{1}{U_c[d_0 + F_A(S-d_0)]} + \frac{1}{C_b} + \frac{R_h}{\pi d_s} + \frac{R_t}{\pi d_s} + \frac{R_s}{\pi d_s}\right]} \quad (11)$$

$$C_{b,\theta} = k_b W/\gamma \quad (12)$$

Where k_b (W/m °C) is the thermal conductivity of the junction, W (m) is the width, and γ (m) is the thickness of the junction between the plate and the tube. Eq(13) is described by the hydraulic diameter ds (m), and x_f (m) is the thickness of the scaling layer.

$$d_s = d_i - 2x_f \quad (13)$$

Additionally, F´ depends on the thermal efficiency of the metal fin (F_A) as given by Eq(14).

$$F_A = \frac{Tanh[M_\theta(S-d_0)/2]}{M_\theta(S-d_0)/2} \quad (14)$$

$$M_\theta = \sqrt{(U_{c,\theta}/(k_{p,\theta})\delta)} \quad (15)$$

ISSN: 2523-6881
RENIECYT-SECIHTI: 1702902

Lugo-Granados, Hebert Gerardo, Canizalez-Dávalos, Lázaro and Picón-Núñez, Martín. [2025]. Análisis comparativo de colectores solares de placa plana evacuados bajo condiciones limpias y de ensuciamiento. Journal Renewable Energy. 9[21] 1-12: e10921112.
https://doi.org/10.35429/JRE.2025.9.21.2.1.12

The terms k_p (W/m°C) and δ (m) represent the thermal conductivity and plate thickness, respectively and the parameter M (m^{-1}), is defined in Eq(15). The overall efficiency (η_f) can be evaluated from Eq(16):

$$\eta_f = \frac{\dot{Q}_u}{I_G A_s} \tag{16}$$

From Equation (17), we can determine the pressure drop within the collector network, which is proportional to the sum of hydraulic resistances K_i (kPa s^2/m^6) and the square of volumetric flow rate $\dot{V}$ (m^3/s).+

$$\Delta P_T = \dot{V}^2 \sum_{i=1}^{n} K_i \tag{17}$$

Equations (18) and (19) represent the main sources of hydraulic resistance. The frictional term, K1 (kPa·s^2/m^6), accounts for pressure losses along the pipe length, while K2 (kPa·s^2/m^6) reflects additional losses caused by fittings such as elbows and valves. Fouling introduces thermal resistance, which in turn affects the overall hydraulic behaviour of the system.

$$K_1 = \frac{8 L_t}{\pi^2 {d_s}^5} f \tag{18}$$

$$K_2 = \frac{8\rho}{\pi^2 {d_s}^5} k_f \tag{19}$$

Here, f denotes the friction factor associated with flow along the pipe, and k_f represents the resistance coefficient for individual fittings. L_t (m) and ds (m) refer to the tube's length and hydraulic diameter, respectively. A reduction in diameter results in greater flow resistance, which in turn causes a higher pressure drop.

2.2 Scaling Simulation

The model proposed by Lugo-Granados and Picón-Núñez (2018) was employed to predict the accumulation of mineral deposits ($CaCO_3$) on the inner walls of the tubes. These deposits affect both the thermal conductivity and the effective flow cross-section. The model is based on prior experimental data obtained from systems operating with hard water, and it enables an assessment of how scaling influences the thermal and hydraulic performance of solar collectors, as shown in Equation (20).

$$\dot{m}_d = \frac{\beta}{2}\left(\frac{\beta}{\alpha k_r} + (C_1 + C_2) - \sqrt{\frac{[\beta + (C_1 + C_2)\,\alpha k_r]^2 + 4\,\alpha^2 {k_r}^2 (K_{sp} - [C_1][C_2])}{\alpha^2 {k_r}^2}}\right) \tag{20}$$

The model calculates the mass flow rate of calcium carbonate deposition, $\dot{m}_d$ (kg/m²·s), within the tubes, based on the key factors that influence scaling. These include the pH of the fluid, the concentrations of calcium ions (Ca^{2+}, denoted as C_1 in kg/m³) and carbonate ions (CO_3^{2-}, denoted as C_2 in kg/m³), as well as the solubility product (K_{sp}) (kg^2/m^6) for $CaCO_3$ in water. Design variables are also considered. Temperature plays a central role, as it affects the rate of the chemical reaction responsible for crystal formation, which is governed by the reaction rate constant k_r (m^2/kg·s). Fluid velocity is another important factor, influencing the rate of deposition through the mass transfer coefficient β (m/s).

The deposition resistance factor α, introduced in Equation (21), is a dimensionless quantity that reflects the influence of viscous and inertial stresses on the adherence of crystals to the surface. This factor was determined from published experimental data. As scaling progresses, it alters the internal surface of the tubes, roughness increases and the effective diameter decreases, leading to a higher pressure drop across the system.

$$\alpha = \frac{191}{f \cdot Re^{1.67}} \tag{21}$$

The thermal resistance due to fouling, Rs (m^2·°C/W), depends on the mass flux of calcium carbonate deposited on the tube surfaces, $\dot{m}_d$, and the rate at which it is removed, $\dot{m}_r$ (kg/m²·s). It also incorporates the density of the deposit, ρ_f (kg/m^3), and its thermal conductivity, λ_f (W/m·°C), as expressed in Equation (22).

$$\frac{dR_s}{dt} = \frac{\dot{m}_d - \dot{m}_r}{\rho_f \lambda_f} \tag{22}$$

The thickness generated by scaling can be determined to by Eq(23).

$$x_f = R_s \lambda_f \tag{23}$$

An economic analysis was carried out considering the following aspects:

ISSN: 2523-6881
RENIECYT-SECIHTI: 1702902

Lugo-Granados, Hebert Gerardo, Canizalez-Dávalos, Lázaro and Picón-Núñez, Martín. [2025]. Análisis comparativo de colectores solares de placa plana evacuados bajo condiciones limpias y de ensuciamiento. Journal Renewable Energy. 9[21] 1-12: e10921112.
https://doi.org/10.35429/JRE.2025.9.21.2.1.12

– Initial costs for both models, including equipment procurement.

– Energy consumption associated with the pumping systems, which is directly affected by the increase in pressure drop.

This approach allows for a comparison not only of thermal and hydraulic performance, but also of the economic and operational feasibility of each collector type. It provides clear criteria for selecting the most suitable option based on the intended application and the quality of the available water.

The total operating cost, $Cost_{total}$ (USD), is obtained by adding the pumping costs, $Cost_p$ (USD), to the annualised cost of the collectors, $Cost_c$ (USD), as indicated in Equation (24). This cost breakdown offers a clearer view of the economic factors involved in running solar thermal systems.

$$Cost_{total} = Cost_p + Cost_c \quad (24)$$

Equation (25) defines the operating cost of the pump, $Cost_p$, which is directly proportional to the unit cost of electricity $Cost_u$, the pumping power $\dot{w}$, and the operating time t, the duration required to reach the target temperature. In this study, the unit cost of electricity is taken as \$0.30 USD/kWh.

$$Cost_p = cost_u \dot{w}\, t \quad (25)$$

The pumping power $\dot{w}$is calculated using Equation (26), based on the pressure drop across the system. It is defined as the product of the volumetric flow rate $\dot{V}$ (m³/s) and the pressure drop ΔP (kPa), divided by the pump efficiency η_b:

$$\dot{w} = \frac{\dot{V}\,\Delta P}{\eta_b} \quad (26)$$

The annualised cost of the collectors, $Cost_c$, is given by Equation (27). It is calculated as the product of the unit cost per collector C_u (USD), the annualization factor Fa, and the total number of collectors Nc. The commercial cost per collector is estimated at \$811.76 USD. To determine the annualization factor Fa, Equation (28) is used. It considers a collector lifespan ω of 20 years and an annual interest rate $\imath$ of 10%:

$$Cost_c = C_u \cdot Fa \cdot N_c \quad (27)$$

$$F_a = \left[\frac{\imath(1+\imath)^{\omega}}{(1+\imath)^{\omega}-1}\right] \quad (28)$$

The simulations assessed the thermohydraulic performance as a function of the number of solar collectors, considering two configurations: flat-plate collectors with parallel tubes and flat-plate collectors with a spiral tube. The system operated under the following conditions:

– Irradiance: 630 W/m²
– Inlet temperature: 20 °C
– Flow rate: 4 L/min
– Water hardness: 250 ppm as $CaCO_3$

A thermal network was designed to reach an outlet temperature of 90 °C. System behaviour was analysed under both clean conditions and after scaling due to mineral deposits, following 4,320 hours of continuous operation.

3.1 Comparison between Collector Configurations

At this stage, the number of collectors required to reach the target temperature was determined. From that point onward, the two configurations (parallel tubes and spiral tube) were compared in terms of thermal efficiency, useful energy transfer, pressure drop, and operating costs.

Box 4

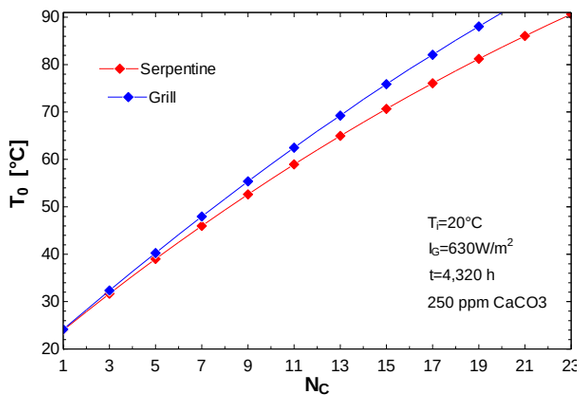

Figure 4
Outlet temperature as a function of the number of collectors for parallel and spiral configurations
Source: Own Elaboration

ISSN: 2523-6881
RENIECYT-SECIHTI: 1702902

Figure 4 illustrates the number of collectors required to reach an outlet temperature of 90 °C under extended operating conditions and in the presence of $CaCO_3$ scaling.

The results show that the parallel-tube configuration requires 20 collectors, whereas the spiral-tube design needs 23 to achieve the same target. This reflects a 13% improvement in efficiency for the parallel arrangement, as fewer collectors are needed. The difference implies lower capital costs, and reduced demands on the pumping system.

Box 5

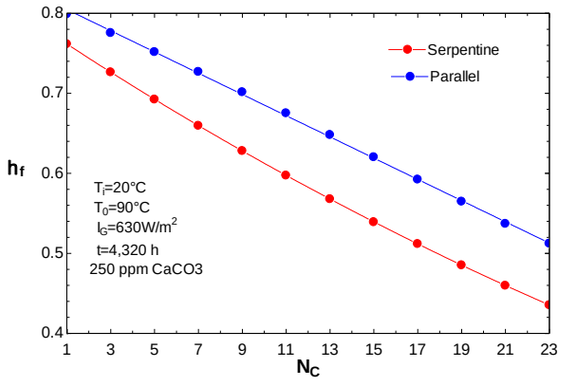

Figure 5

Thermal efficiency as a function of the number of installed solar collectors

Source: Own Elaboration

Figure 5 shows how thermal efficiency varies with the number of solar collectors for the two configurations: parallel tubes and spiral tubes.

With a single collector, the parallel-tube setup reaches an efficiency of 0.80, while the spiral-tube design achieves 0.76. However, as the number of collectors increases to 20, both efficiencies decline due to greater thermal losses and the cumulative effect of fouling.

At that point, efficiency drops to 0.55 for the parallel arrangement and to 0.48 for the spiral configuration—corresponding to reductions of 31.25% and 36.84%, respectively. Moreover, at the upper end of the range, the parallel configuration maintains an efficiency approximately 14.6% higher than that of the spiral design. This suggests that the parallel layout not only performs better initially but also retains superior efficiency as the system scales.

Box 6

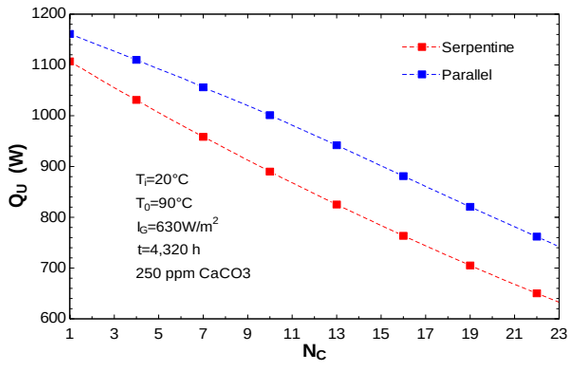

Figure 6

Comparison of thermal load according to the number of solar collectors

Source: Own Elaboration

Figure 6 illustrates the relationship between thermal load and the number of solar collectors for two configurations. Although thermal load decreases linearly with the number of collectors in both cases, the parallel-tube configuration consistently delivers better thermal performance.

As shown in the graph, the parallel collectors (blue line) outperform the spiral ones (red line), with the gap widening as the system grows. For instance, with two collectors, the parallel setup delivers approximately 70 W more than the spiral, representing a 7.14% improvement. With eight collectors, the difference increases to 100 W, equivalent to a 10.6% gain in thermal load.

This trend suggests that the parallel design is not only more efficient under extended operating conditions and calcium carbonate fouling, but its advantage becomes increasingly pronounced as the collector network expands.

Box 7

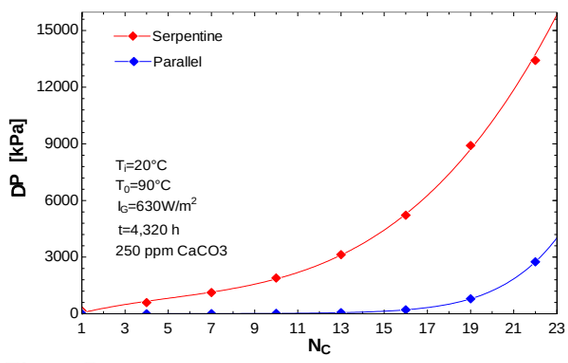

Figure 7

Variation in pressure drop with respect to the number of collectors in both configurations

Source: Own elaboration

ISSN: 2523-6881
RENIECYT-SECIHTI: 1702902

Lugo-Granados, Hebert Gerardo, Canizalez-Dávalos, Lázaro and Picón-Núñez, Martín. [2025]. Análisis comparativo de colectores solares de placa plana evacuados bajo condiciones limpias y de ensuciamiento. Journal Renewable Energy. 9[21] 1-12: e10921112.
https://doi.org/10.35429/JRE.2025.9.21.2.1.12

Figure 7 shows how pressure drop varies with the number of connected solar collectors. As more collectors are added, the pressure drop increases due to the longer fluid path and greater frictional losses.

A clear distinction emerges between the two configurations. Collectors with spiral tubes (red line) exhibit significantly higher pressure losses compared to those with parallel tubes (blue line). For instance, with 20 collectors, the pressure drop in the spiral arrangement reaches approximately 11,000 kPa, whereas the parallel setup registers only 1,000 kPa, a reduction of 90.9% when opting for the parallel configuration.

Figure 8 presents the system cost as a function of the number of collectors. Like the pressure drop, total cost rises with the number of units, as both parameters are closely linked.

For example, with 20 collectors, the estimated cost for the spiral configuration is $500, while the parallel arrangement amounts to just $100. This translates into a cost saving of 83.3% when choosing the parallel-tube design.

Box 8

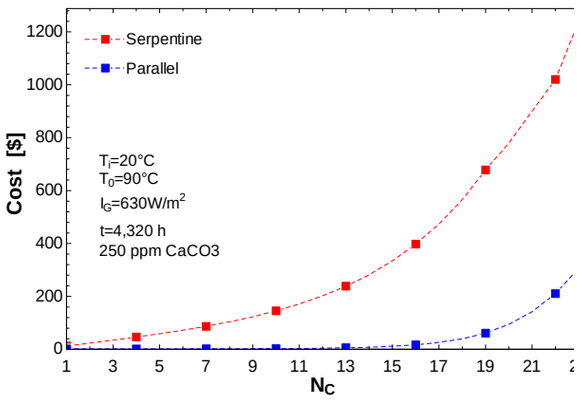

Figure 8

Cost comparison based on the number of connected collectors for each technology

Source: Own Elaboration

2.2 Comparison under Clean and Fouled Conditions

This section presents the results of the analysis for four solar collector configurations:

1. Spiral arrangement with 23 collectors under clean conditions (23s_S(NF))
2. Spiral arrangement with 23 collectors affected by fouling (23s_S(F))
3. Parallel arrangement with 20 collectors under clean conditions (20s_G(NF))
4. Parallel arrangement with 20 collectors affected by fouling (20s_G(F))

These configurations allow for a comparative assessment of thermal performance and system efficiency under varying operational conditions.

Box 9

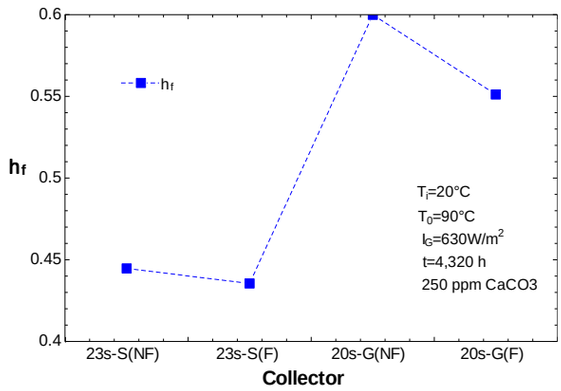

Figure 9

Efficiency comparison by collector type, under clean and scaled conditions

Source: Own Elaboration

From a thermal standpoint (Figure 9), the parallel configuration demonstrates higher efficiency in reaching the target temperature of 90 °C. Under clean conditions, spiral collectors reach an efficiency of 0.44, whereas the parallel arrangement achieves 0.60, an improvement of 36.4%. Although both configurations experience efficiency losses due to scaling, the impact is notably more severe in the spiral design.

Box 10

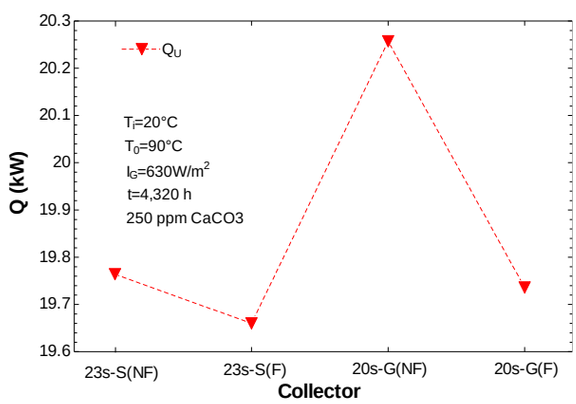

Figure 10

Instantaneous thermal load by collector type, under clean and scaled conditions.

Source: Own Elaboration

ISSN: 2523-6881
RENIECYT-SECIHTI: 1702902

Lugo-Granados, Hebert Gerardo, Canizalez-Dávalos, Lázaro and Picón-Núñez, Martín. [2025]. Análisis comparativo de colectores solares de placa plana evacuados bajo condiciones limpias y de ensuciamiento. Journal Renewable Energy. 9[21] 1-12: e10921112.
https://doi.org/10.35429/JRE.2025.9.21.2.1.12

Figure 10 presents the results for instantaneous thermal load, which follow the same trend observed in efficiency. The clean spiral setup (23s_S(NF)) delivers 19.78 kW, dropping slightly to 19.67 kW with fouling (23s_S(F)). In contrast, the clean parallel configuration (20s_G(NF)) reaches 20.25 kW, decreasing to 19.75 kW under fouled conditions (20s_G(F)). These results confirm that hydraulic design directly influences the recovery of useful energy, and that the parallel configuration is more resilient to the effects of scaling.

Box 11

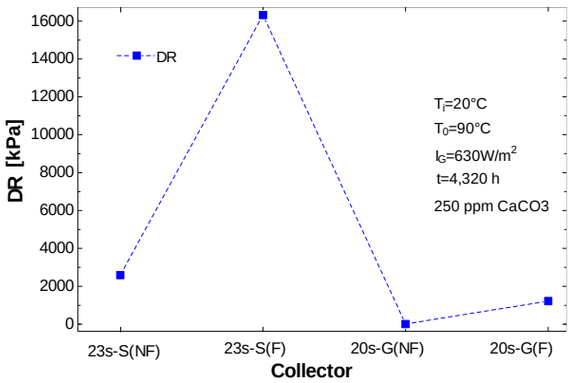

Figure 11

Pressure drop comparison by collector type, with and without scaling

Source: Own Elaboration

Figure 11 compares pressure drop (ΔP) across collector types, with and without fouling. In the clean spiral setup (23s_S(NF)), the pressure drop is 2,600 kPa, rising sharply to 16,000 kPa with scaling (23s_S(F)), a 515% increase. The parallel configuration shows much lower values: 300 kPa under clean conditions (20s_G(NF)) and 1,200 kPa when fouled (20s_G(F)), representing a 300% increase. This contrast highlights the hydraulic advantages of parallel design, particularly in scenarios involving mineral deposit accumulation.

Finally, Figure 12 presents the operating costs associated with both configurations. These follow a similar trend to the pressure drop, as pump energy consumption is directly linked to hydraulic resistance. In the presence of scaling (F), costs rise significantly. For the parallel setup (20s_G), the increase is 196%, while for the spiral configuration (23s_S), it reaches 500%.

Box 12

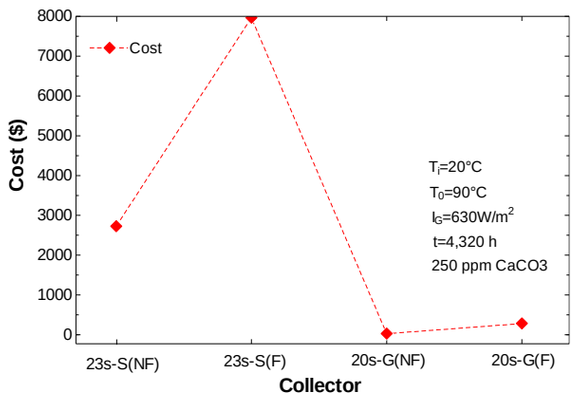

Figure 12

Cost comparison by collector type, with and without scaling

Source: Own Elaboration

Despite the percentage increase in operating costs due to scaling, collectors with parallel-tube configuration maintain significantly lower overall costs. Under clean conditions, the savings exceed $2,500, and in the presence of fouling, they can reach up to $7,500. This positions them as a more cost-effective and efficient alternative, both hydraulically and energetically.

3. Conclusions

The results of this study demonstrate that the evacuated flat-plate solar collector with parallel-tube configuration offers superior performance in terms of thermal efficiency, hydraulic behaviour, and operating costs when compared to the spiral-tube design. This technology performs reliably at low and medium temperatures and retains its efficiency even under scaling conditions, making it well-suited for long-term, real-world applications.

Its favourable performance is attributed to the multi-path parallel design, which promotes better fluid distribution and lower pressure drop, thereby enhancing heat transfer even under adverse conditions. In contrast, spiral configurations, with a single extended flow path, exhibit higher hydraulic resistance and are more vulnerable to performance losses due to scaling. For prolonged operation and in environments with high water hardness, the parallel-tube layout proves to be more efficient and dependable. Moreover, the higher thermal efficiency of the parallel design allows energy targets to be met with fewer modules, resulting reduced capital investment, and lower pumping requirements.

ISSN: 2523-6881
RENIECYT-SECIHTI: 1702902

Lugo-Granados, Hebert Gerardo, Canizalez-Dávalos, Lázaro and Picón-Núñez, Martín. [2025]. Análisis comparativo de colectores solares de placa plana evacuados bajo condiciones limpias y de ensuciamiento. Journal Renewable Energy. 9[21] 1-12: e10921112.
https://doi.org/10.35429/JRE.2025.9.21.2.1.12

The comparative analysis of spiral and parallel solar collector configurations, under both clean and scaled conditions (250 ppm $CaCO_3$), leads to the following specific conclusions:

- **Thermal Performance:** The parallel configuration without scaling (23s-G(NF)) achieved the highest thermal efficiency and useful load, reaching 20.25 kW, outperforming the spiral designs. Although scaling affected both configurations, the impact was more pronounced in the spiral collectors.

- **Hydraulic Performance:** Marked differences in pressure drop were observed. Spiral collectors reached up to 16,000 kPa under scaled conditions, a 515% increase compared to their clean state. In contrast, parallel collectors showed a much lower pressure drop (1,200 kPa), even with fouling, indicating a more favourable hydraulic response.

- **Economic Performance:** Operating cost variations were directly linked to pressure drop. Under scaling conditions, the spiral configuration's operating cost increased by up to 500%, while the parallel setup exhibit a rise of 196%. Nevertheless, parallel collectors maintained the lowest costs in both scenarios.

In summary, solar collectors with parallel-tube configuration offer clear advantages in thermal efficiency, hydraulic behaviour, and operating costs, even under scaling conditions. Their design supports better fluid distribution and reduced resistance, making them a more reliable and cost-effective option for extended use. Their implementation is recommended in settings with high water hardness, where spiral configurations face significant operational limitations.

Technical Recommendation

This study confirms that parallel-tube solar collectors provide notable benefits in thermal, hydraulic, and economic terms. They exhibit lower sensitivity to fouling and maintain stable, efficient performance over time.

For this reason, their use is advised in long-duration applications and in conditions prone to scaling. Additionally, the adoption of preventive cleaning schemes is recommended to preserve system performance.

Declarations

Conflict of interest

The authors declare no interest conflict. They have no known competing financial interests or personal relationships that could have appeared to influence the article reported in this article.

Author contribution

Lugo-Granados, Hebert Gerardo: Contributed to the research methodology and generation of results and writing of the manuscript.

Canizalez-Dávalos, Lázaro: Contributed to the research method and revision of the manuscript.

Picón-Núñez, Martín: Contributed to the project idea, research method, editing and revising of the manuscript.

Funding

This work has been funded by SECIHTI [grant number 2466286,487049].

Abbreviations

A_c	Collector area 2.506 (m^2)
A_s	Plate area (m^2)
C_1	Ca^{2+} concentration(kg/m^3),
C_2	CO_3^{2-} concentration(kg/m^3)
C_b	Thermal resistance between tube and plate (m^2 °C/W)
$Cost_a$	Annualised cost of solar collector ($/year)
$Cost_b$	Operating cost ($)
$Cost_t$	Total operating cost ($)
$cost_u$	Unit cost of electricity ($/kwh)
Cp	Water heat capacity (kJ/kg °C)
C_u	Commercial cost of a solar collector ($811.76 dollars)
d_0	Collector tube outer diameter (m).
d_i	Collector tube inner diameter (m)
d_s	Hydraulic diameter (m)
f	Friction factor
$F´$	Collector efficiency factor
F_A	Metal fin thermal efficiency
Ƒa	Annualization factor
F_R	Heat removal factor

ISSN: 2523-6881
RENIECYT-SECIHTI: 1702902

i	Interest rate (8%)
I_G	Solar radiation (W/m^2)
K_1	Friction resistance (kPa s^2/m^6)
K_2	Hydraulic resistance due to connections (kPa s^2/m^6)
k_b	Thermal conductivity (W/m °C)
k_r	Reaction constant (m^2/kg s)
k_f	Resistance factor
K_s	Thermal conductivity of plate (W/m °C)
K_{sp}	$CaCO_3$ solubility (kg^2/m^6)
L_t	Tube length (m)
$\dot{m}_d$	Mass flux (kg/m^2 s)
$\dot{m}_f$	Mass flow rate (kg/s)
$\dot{m}_r$	Mass flux removed (kg/m^2 s
Nc	Total number of collectors
Q	Process thermal load
Q_u	Useful heat (kW)
Q_T	Total heat load (kW)
Re	Reynolds number
R_h	Thermal resistance due to convection (m^2 °C/W)
R_s	Thermal resistance due to fouling (m^2 °C/W)
R_t	Thermal resistance due to conduction (m2 °C/W),
S	Distance between tubes (m)|
t	Operating time (h).
T_0	Outlet temperature (°C)
T_a	Ambient temperature (°C)
T_i	Inlet temperature (°C)
T_{pm}	Plate temperature (°C)
U_c	Overall heat transfer coefficient of losses (W/m^2°C)
W	Width (m)
x_f	Fouling layer thickness (m)
$\dot{V}$	Volumetric flow rate (m^3/s)
ΔP	Pressure drop (kPa)
$\dot{w}$	Pumping power
α	Deposition resistance factor
α_c	Plate absorbance
β	Mass transfer coefficient (m/s)
γ	Thickness between plate and tube (m)
δ	Plate thickness (m)
η_f	Collector thermal efficiency
η_b	Pump efficiency
ï	Annual interest rate
Λf	Thermal conductivity of $CaCO_3$ (W/m °C)
ρ	Density of water (kg/m^3)
ρf	Density of $CaCO_3$ (kg/m^3)
τ	Cover transmittance
ω	Collector lifespan of 20 years

References

Antecedents

Ayompe, L. M., Duffy, A., McCormack, S. J., McKeever, M., & Conlon, M. [2011]. Comparative field performance study of flat plate and heat pipe evacuated tube collectors (ETCs) for domestic water heating systems in a temperate climate. Energy. 3370–3378.

Kalair, A. R., Seyedmahmoudian, M., Saleem, M. S., Abas, N., Rauf, S., & Stojcevski, A. [2022]. A comparative thermal performance assessment of various solar collectors for domestic water heating. International Journal of Photoenergy. 9536772.

Kalogirou, S. A. [2004]. Solar thermal collectors and applications. Progress in Energy and Combustion Science. 231–295.

Basics

Deng, Y., & Zhao, Y. [2013]. Experimental investigation of performance for the novel flat-plate solar collector with micro-channel heat pipe array (MHPA-FPC). Applied Thermal Engineering. 440–449.

Gao, D., Gao, G., Cao, J., Zhong, S., Ren, X., Dabwan, Y. N., Hu, M., Jiao, D., Kwan, T. H., & Pei, G. [2020]. Experimental and numerical analysis of an efficiently optimized evacuated flat plate solar collector under medium temperature. Applied Energy. 115129.

Hassan, Z., Mahmood, M., Ahmed, N., Saeed, M. H., Khan, R., Abbas, M. M., Kalam, M. A., Almomani, F., & Abdelsalam, E. [2023]. Techno-economic assessment of evacuated flat-plate solar collector system for industrial process heat. Energy Science & Engineering. 2185–2201.

Pandey, K. M., & Chaurasiya, R. [2017]. A review on analysis and development of solar flat plate collector. Renewable and Sustainable Energy Reviews. 641–650.

Supports

Bott, T. R. (1995). Fouling of heat exchangers. Elsevier. Chemical Engineering Monographs. 97-135.

ISSN: 2523-6881
RENIECYT-SECIHTI: 1702902

Lugo-Granados, Hebert Gerardo, Canizalez-Dávalos, Lázaro and Picón-Núñez, Martín. [2025]. Análisis comparativo de colectores solares de placa plana evacuados bajo condiciones limpias y de ensuciamiento. Journal Renewable Energy. 9[21] 1-12: e10921112.
https://doi.org/10.35429/JRE.2025.9.21.2.1.12

Duffie, J. A., & Beckman, W. A. [2013]. Solar engineering of thermal processes. 4th edition. Wiley. 236-319.

Lugo-Granados, H., Picón Núñez M. [2018]. Modelling scaling growth in heat transfer surfaces and its application on the design of heat exchangers. Energy, 845-854.

Lugo-Granados, H. G., Canizalez-Dávalos L., Picón-Núñez Martín. [2023]. Thermohydraulic effects of scaling in flat plate solar collector networks. Chemical Engineering Transactions, 103, 421–426.

Lugo-Granados H. G., Picón-Núñez M., Canizalez-Dávalos L. [2024]. Flat plate solar collector networks: Design and retrofit considering fouling effects. Thermal Science and Engineering Progress. 102633.

Discussions

Bocanegra, J. A., Marchitto, A., & Misale, M. [2025]. Nanofluids in solar collectors: A comprehensive review focused on its sedimentation. Clean Technologies and Environmental Policy. 1753–1784.

Deshmukh, K. Bhausaheb, Nehe, S., Sargar, T., Benschwartz, R., Varkute, N., Vengadesan, E. and Karmare, S. [2025]. Heat Transfer, Friction Factor, and Performance Evaluation of U-Pipe Evacuated Tube Solar Thermal Collector with TiN Nanofluid and Twisted Tape Inserts. Journal of Renewable Energy and Environment. 40-59.

García-Rincón, M. A. & Flores-Prieto, J. J., [2024]. Nanofluids stability in flat-plate solar collectors: A review. Solar Energy Materials and Solar Cells. 112832.

ISSN: 2523-6881
RENIECYT-SECIHTI: 1702902

Lugo-Granados, Hebert Gerardo, Canizalez-Dávalos, Lázaro and Picón-Núñez, Martín. [2025]. Análisis comparativo de colectores solares de placa plana evacuados bajo condiciones limpias y de ensuciamiento. Journal Renewable Energy. 9[21] 1-12: e10921112.
https://doi.org/10.35429/JRE.2025.9.21.2.1.12